Surface modification of cellulose nanowiskers with organosilane to fabricate high-performance polylactic acid nanocomposite materials

Yongqi Yu, Jiaojiao Miao, Zhaodong Ding, Xuejiao Liu, Xuan Wang, Liping Zhang*

MOE Engineering Research Center of Forestry Biomass Materials and Bioenergy, Beijing Forestry University, Beijing, 100083, China, email: yuyq2016@163.com (Y. Yu), mjj.smile@163.com (J. Miao), dzdhero@163.com (Z. Ding), 2436194688@qq.com (X. Liu), 578609319@qq.com (X. Wang), zhanglp418@163.com (L. Zhang)

ABSTRACT

Cellulose nanowisker (CNW) treated by organosilane (aminopropyltriethoxysilane (APS)) reinforced polylactic acid (PLA) via solvent casting evaporation process were developed. The effects of APS concentration and modified nanocellulose content in the nanocomposites were investigated. APS modified CNW (designated as A-CNW) was confirmed using Fourier transform infrared spectroscopy (FTIR), transmission electron microscopy (TEM) and X-ray photoelectron spectroscopy (XPS) measurements, which provided further evidences about the efficiency of CNW surface modification. Nanocomposites were prepared by casting the N, N-dimethylacetamide (DMAc) solutions onto glass plates and evaporating the solvent at 80°C. The interfacial adhesion between CNW and PLA was obviously improved, which can be clearly observed by scanning electron microscope (SEM) analysis. Tensile properties and thermal/dynamic mechanical thermal properties of the composites were studied theoretically and experimentally to see how APS concentration and CNW content affected the resulting PLA/A-CNW nanocomposites. The tensile strength and elongtion increased from 35.7 MPa to 50.6 MPa and from 2.5% to 5.2%, respectively, for nanocomposites with 2% v/v APS and 3 wt % CNW. Dynamic mechanical thermal analysis revealed a decrease in damping and an increase in storage modulus for treated nanocomposites. The presence of A-CNW favored its dispersion in the PLA matrix.

Keywords: Polylactic acid; Cellulose nanowiskers; Organosilane treatment; Nanocomposites; Solvent casting evaporation process

1. Introduction

Polylactic acid (PLA), derived from renewable resources [1], has been the frontrunner in those biodegradable and recyclable biopolymers [2] because of its attractive mechanical properties, renewability and relatively low cost [3,4]. With good processability [5] and recyclability, PLA shows great potential for the applications in industrial plastic, automotive and biomedical fields [6,7], however, the properties of PLA such as the brittleness [8], low impact strength and low thermal stability [1] related to its drawbacks make its usage limited. To overcome these disadvantages, a solution has largely developed over the past years involved in incorporating nano-sized reinforcing elements within the PLA matrix [6,9–11]. In this respect, cellulose nanowiskers (CNWs) represent promising nanofiller with the excellent mechanical properties (e.g., Young's modulus of about 150 GPa), sustainability [8] biodegradability and high surface-reactivity (from hydroxyl functions). They have been obtained by diluted acid hydrolysis of wood pulpboard and homogenizing process [12,13]. They offer greater opportunities to develop a new class of light-weight, transparent and enviromental friendly nanocomposites.

Fine nanofiller dispersion within the polymeric matrix is crucial to develop polymeric nanocomposites with outstanding properties. CNWs reveal a defect in reinforcing the polymeric matrix that is the strong hydrophilic nature due to large amount of hydroxyl groups, which causes low compatibility and poor interfacial adhesion with polymeric

---

*Corresponding author.

matrices [14]. Poor interfacial adhesion leads to an inefficient stress tranfer under load, resulting in low mechanical strength [15,16]. In order to improve their compatibility, CNWs are currently modified via the reaction between the hydroxyl groups located at their surface. Several studies have been reported using surfactant (polarheads and long hydrophobic tails), compatibilizer and polymer chains grafted through "grafting from" and "grafting onto" methods [17–20]. Nevertheless, the surface-functionalization is not straightforward and enviromentally-friendly due to the adsorption of organic solvents. Direct surface-functionlization starting from aqueous CNW suspension seems to be an efficient way to solve these issues.

In this regard, silanes are recognized as efficient coupling agents extensively used in composites and adhesive formulations [21]. Functional trialkoxysilanes (R'Si(OR)$_3$) are widely used in water as coupling agents via hydrolysis and condensation reactions to enhance the adhesion between polymeric matrices and CNWs [22,23], which have been successfully applied in inorganic filler such as glass fiber and mineral [24,25]. They have also been applied in natural fiber/polymer composites due to their bio-functional structures, since both glass fibers and natural fibers bear reactive hydroxyl groups. In the present work, we proposed to surface-functionalize CNWs in the presence of aminopropyltriethoxysilane (APS) and use the APS treated CNW (A-CNW) as nanofillers in PLA-based nanocomposite films. The effects of APS and the addition of CNW on the properties of PLA matrix were investigated. FTIR, XPS and TEM analyses were used as characterization tools for A-CNWs. Then, A-CNWs were blended with PLA using a solvent casting method. The fracture-surface morphology was observed by SEM analysis. DMA and DSC were carried out to investigate the thermomechanical properties of the resulting nanocomposite films, and compared with neat PLA. Tensile properties of the nanocomposite films were also presented in this article. The objective of this work was to examine the effects of surface treatment of CNW on the dispersion of CNW and the mechanical properties of the resulting PLA nanocomposite films.

2. Materials and methods

2.1. Materials

Lignocellulose pulpboard was obtained from Huatai paper mill, Shandong, China. Sulfuric acid, acetic acid and N, N-dimethylacetamide (DMAc) from Beijing Chemical Plant were used as-received. Aminopropyltrimethoxysilane (APS) from Beijing shenda fine chemical Co., Ltd was used as-received. A biodegradable, thermoplastic matrix PLA (M_w = 100,000) was purchased from Shanghai Yisheng industry Ltd.

2.2. Organosilanization of CNWs

The CNWs were achieved base on the previous literature [13]. In a 250 ml flask, a CNW suspension (1 g CNWs in 100 mL 80/20 v/v ethanol/distilled water) was placed at pH of 4 by adding acetic acid into it. Then, APS was added into the suspension, followed by a stirring for 2 h at ambi-

ent temperature. The CNWs were then washed twice by tap water, and then washed several times with DMAc. The 1%, 2%, 5% of APS modified CNWs (volume percentage of APS to the CNW suspension: v/v) were studied in the research.

The A-CNW solid was dispersed in DMAc, ultrasonicated for 20 min at a frequency of 40 Hz (KQ 5200DB, China), then the suspension of A-CNW dispersed in DMAc was obtained.

2.3. Nanocomposites preparation

The desired amount of PLA was added into A-CNW suspension, and then stirred at 80°C for 2 h. The suspension (Table 1) was poured onto a glass and scraped. The composites were cured at 80°C for 10 min and post cured under vacuum condition at 40°C for 24 h to ensure that the solvent had completely evaporated. The thickness of films was approximately 150 μm.

2.3. Characterization

Fourier transform infrared (FTIR) spectra were recorded using a Tensor 27 (Bruker, Germany) device with an ATR Harrick Split Pea. Spectra were recorded using a spectral width ranging from 4000 to 400 cm^{-1}, with 2 cm^{-1} resolution and an accumulation of 32 scans.

The morphology of the nanocomposites was recorded using a transmission electron microscope, TEM (Jem 2100 HRTEM, acceleration voltage 80 kV). Differential scanning calorimetry (DSC) analysis was performed using a TA Instruments Q200 apparatus. A heat/cool/heat procedure was applied for a temperature range from 25°C to 200°C with a rate of 10°C/min.

Thermomechanical properties of the nanocomposites were performed under ambient atmosphere using a Q800 DMTA apparatus from TA Instruments using a dual cantilever module. The measurements were carried out at a constant frequency of 1 Hz and an amplitude of 5 μm, following a temperature range from 0 to 100°C for PLA based materials at a heating rate of 5°C/min.

Mechanical tests of nanocomposites were conducted on a DCP-KZ300 at a crosshead speed of 20 mm/min, according to the European Standard NF-EN-ISO-527-3:1995. Samples for mechanical analysis were prepared with dimensions of approximately 15 mm × 100 mm. The mechanical tests were

Table 1
Formulation and sample code for the nanocomposites investigated in this study

Samples	PLA concentration (wt%)	APS concentration (v/v %)	A-CNW concentration (w/w %)
PLA	16	0	0
PLA-AC1	16	1	3
PLA-AC2	16	5	3
PLA-AC3	16	2	1
PLA-AC4	16	2	3
PLA-AC5	16	2	5

carried out with five individual films for each of the casting solution, and the average value was taken as the datum point.

The fracture surface of nanocomposites was studied with a JSM5900 scanning electron microscope (SEM) under an accelerating voltage of 5 kV. All the surfaces were sputtered with gold. In addition, X-ray photoelectron spectroscopy (XPS, ESCALAB 250Xi, 1eV per step and 0.05 eV per step for narrow scan) was used to study the surface compositions of A-CNW. The XPS experiments were conducted at room temperature with a base pressure of 10^{-9} mbar.

3. Results and discussions

3.1. Mechanism of APS modified CNW reinforcing PLA

The reaction process of organsilanization which takes place in cellulose surface is shown in Fig. 1. Firstly, the alkoxy groups of APS reacted with water to form silanol and the concomitant condensation of silanols took place. Then a small molecular size of oligomers were retained to diffuse into the cellulose surface, the reactive oligomers and hydroxyl groups on the glucose units of the cellulose leading to hydrogen bonded on the fiber surface. When combined with the PLA matrix, a reaction between amine groups from APS and acid end groups of PLA led to the formation of an amide function. Chemical bonding could be established between the CNW and PLA matrix, and interfacial properties could be improved.

3.2. FTIR characterization

The FTIR spectra of untreated and treated CNW are presented in Fig. 2. FTIR spectrum clearly showed the appearance of the peaks corresponding to CNW: the broad band at 3600–3200 cm^{-1} can be assigned to free OH groups of cellulose molecules. The absorption peak around 2900 cm^{-1} was due to stretching of C-H grou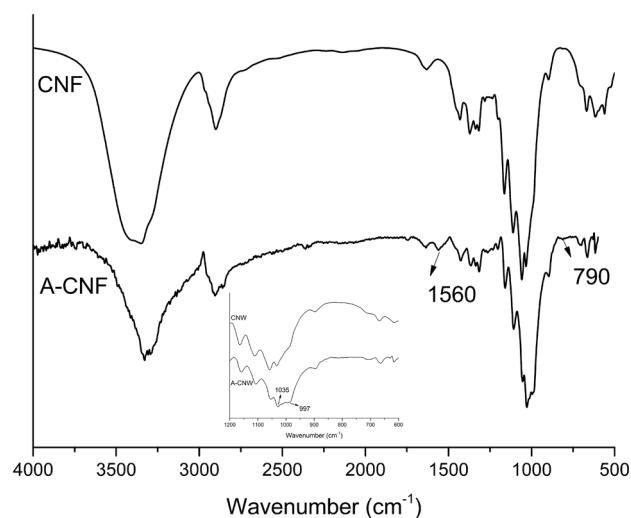ps. The peak at around 1635 cm^{-1} was probably associated with absorbed water in crystalline cellulose [16]. The peak at 1432 cm^{-1} was attributed to CH_2 bending stretching, and 1371 cm^{-1} to C-H. The absorption peaks at 1058 cm^{-1} and 1035 cm^{-1} were related to the C-O stretching, the peak located at 900 cm^{-1} was corresponding to the C-H bending or $-CH_2$ stretching which indicated the amorphous structure of CNW [26,27].

The results showed that APS treated CNW after drying at room temperature overnight exhibited the band at 1560 cm^{-1} which was typical of amino group that was strongly hydrogen bonded to the hydroxyl groups of silanol in agreement with the Abdelmouleh et al. [28] study. The weak band at 997 cm^{-1} was assigned to the unreacted silanol groups produced in the silane hydrolysis [27]. The strong absorption of cellulose bond in the region of 1000–1200 cm^{-1} made it difficult to completely assign to the Si-O-Si and Si-O-C$_{cellulose}$ [29]. The intensity of the peak at 1035 cm^{-1}, which was an overlap of Si-O-Si band and the C-O stretching of cellulose, was increased after APS treatment, further evidence of silane adsorption [27].

3.3. XPS analysis

The elemental compositions of CNW and A-CNW obtained from the XPS spectra are shown in Fig. 3A, and the relative atomic concentration and oxygen-to-carbon ratios are summarized in Table 2. The CNW had the oxygen-to-carbon (O/C) atomic ratio of 0.71, which was slightly below the theoretical O/C value of 0.83 for pure cellulose, possibly because of the presence of C-rich molecular segments at the surface of the solids under study. This difference could be attributed to the surface pollution by hydrocarbons adsorbed at the surface of nanofibers [30]. For A-CNW, the presence of silicon and nitrogen was determined, indicating clearly the bonding of silane to CNW. Meanwhile, the ratio of O/C decreased from 0.71 to 0.55, with the silane treatment due to the bonding of APS.
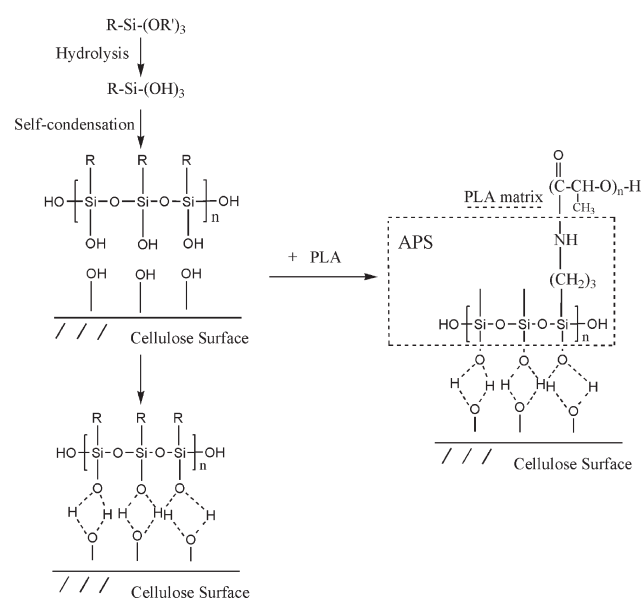

Fig. 1. The reaction mechanism of APS on the cellulose surface and the reinforcing mechanism of A-CNW/PLA nanocomposite.

Fig. 2. The FT-IR spectra of untreated and APS treated CNW.
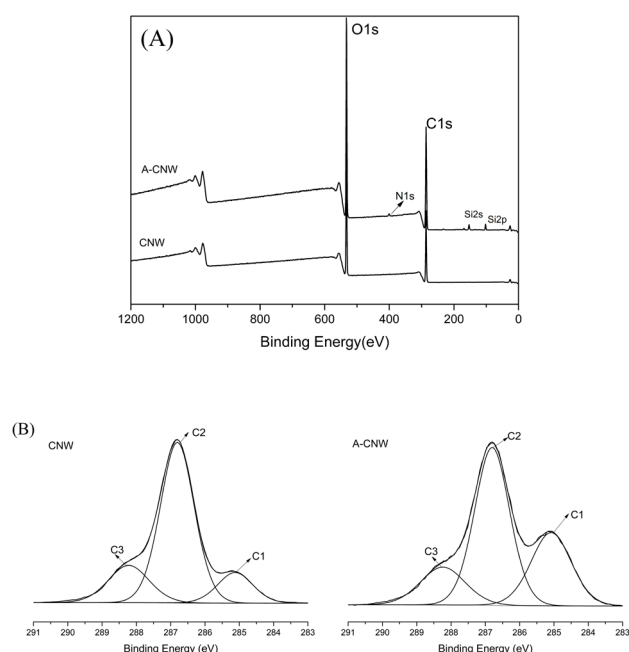
Fig. 3. XPS spectrum of CNW and A-CNW (A) and the high solution C1s spectra (B).

Table 2
The atomic concentration of CNW and APS treated CNW

	O/C	C1s	O1s	N1s	Si2p
CNW	0.71	58.09	41.62		
A-CNW	0.55	61.94	34.15	0.87	3.04

Table 3
Relative carbon composition of CNW before and after APS treatment

	C1(C-C)	C2(C-O)	C3(C-O-C)
CNW	13.36	67.80	18.85
A-CNW	28.93	54.48	16.59

The high solution C1s spectra of the CNW and A-CNW are shown in Fig. 3B, in the case of the C_{1s} spectra of CNW, it shows the presence of three types of carbon bonds: C-C (C1, 285 eV), C-O (C2, 286.7 eV), and C-O-C (C3, 288.3 eV) [31]. These results are summarized in Table 3. The intensity of the C1 peak increased from 13.36% for CNW up to 28.93% for the APS treated CNW, which was due to the presence of the propyl groups of APS. In addition, the intensity of the C2 and C3 peaks decreased. It was demonstrated that APS displayed a better adsorption affinity toward the CNW substrate.

3.4. TEM analysis of CNW and A-CNW

The size distribution and morphology of the CNWs were analyzed by TEM and the results are exhibited in Fig. 4. It was difficult to determine the size of CNW due to agglomeration, but from several images the CNW presented the typical dimensions of aspect ratio from 20 to 50. The average diameter of A-CNW (ca. 50 nm) was higher than those of neat CNW (ca. 25 nm), which was more likely relied on the formation of a polysiloxane layer onto the A-CNW surface after silanization. Also, the result was consistent with the FTIR and XPS that the APS couple agent was successfully grafted onto CNW. The A-CNW kept the integrity and rod-like structure, which can be used as nanoreinforcing agent for polymer matrix.

3.5. Mechanical properties

Tensile properties have been evaluated for neat PLA and PLA/A-CNW composite films. Fig. 5 shows the changes of mechanical properties of the PLA (100%)/ silanized CNW (3%) composites films with various contents of APS silane agents. The results showed that the

CNWs treated with APS can improve the tensile strength and elongation at break obviously. The composite film with 2% v/v silanized CNWs showed the best tensile properties, the tensile strength and elongation increased significantly by 42.8% (50.6MPa) and 108% (5.2%), in comparison with the neat PLA film whose tensile strength and elongation were 35.7 MPa and 2.5%, respectively. In addition, the tensile strength dropped drastically with 5% v/v APS content. This mechanical behavior was due to the improvement of CNW/PLA adhesion when CNW was modified with organosilane (APS). The increase of tensile strength may be attributed to the chemical bond between PLA matrix and amino groups linked to the cellulose surface [16]. At the 5%v/v APS, the interface strength would exceed the native strength of the CNW itself. Therefore, the break of the CNW occurred under the tensile loading, leading to the crack initiation.

The mechanical behavior for composite films reinforced with 1, 3, 5 wt % of 2% v/v APS modified CNW was performed by tensile testing at room temperature, respectively. Fig. 6 shows the effect of A-CNW content on the tensile strength and elongation. The figure clearly showed that increased A-CNW content had positive effect on composite films strength compared to neat PLA. By incorporating 3 wt% A-CNW, composites had the highest tensile strength, increased by 42.8% compared to pure PLA. When adding 1 wt% content of A-CNW, there was not enough A-CNW to cross with each other and form a network in the PLA matrix. However, the strong self-aggregating nature of A-CNW (5 wt %) led to a less pronounced increase in tensile strength. The interfacial adhesion between A-CNW and PLA weakened.

The ever-increasing improvement in tensile strength can be attributed to the improvement in the surface chemical compatibility between CNW and the PLA matrix after silanization. The tensile results indicated that the addition of APS can promote the reinforcement of CNW/PLA composites. The tensile strength of composite films firstly increased and then decreased with the increase of APS concentration or A-CNW content in PLA matrix. The reason may be that more APS underwent self-condensation and form hydroxyl bond among APS, which made the layer between PLA and CNW too thick and led to the difficulty in stress-transferring. The self-aggregated nano-size filler could be adopted
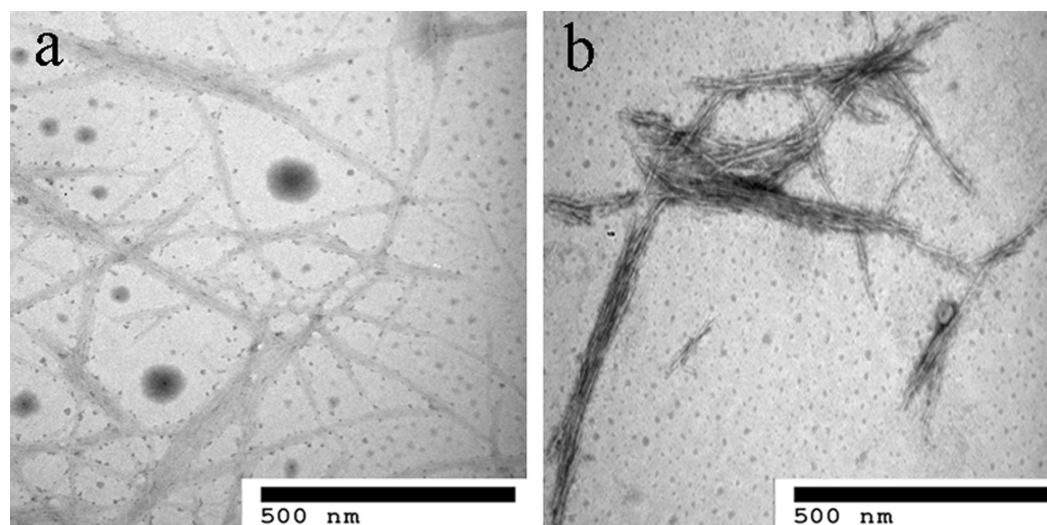
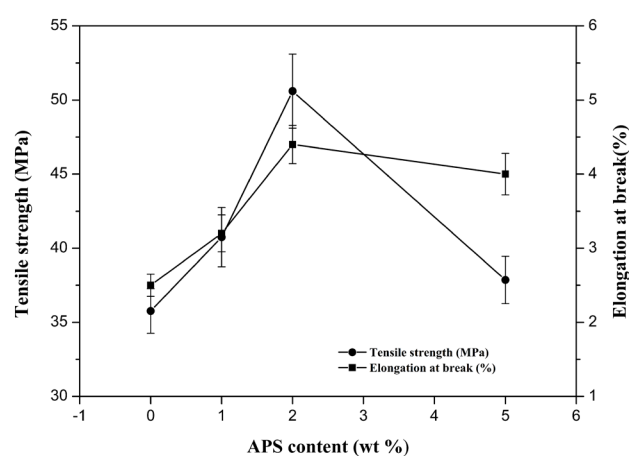Fig. 4. TEM images of CNWs (a) and A-CNWs (b).

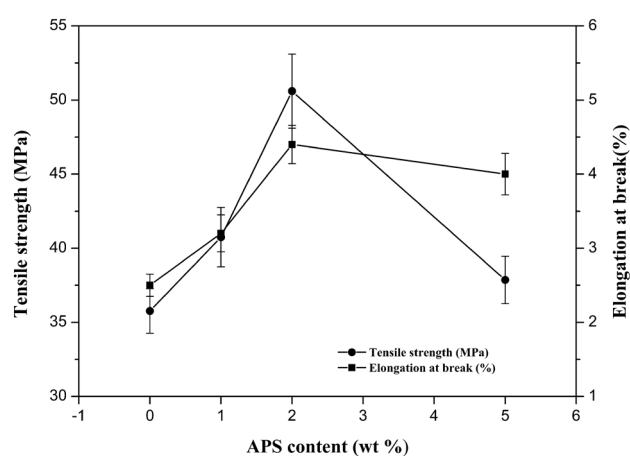Fig. 5. The effect of APS content on mechanical properties of nanocomposites.

Fig. 6. The effect of A-CNW content on mechanical properties of nanocomposites.

to explain why more A-CNW adding would decrease the mechanical properties of PLA matrix.

3.6. DSC analysis

The thermal behavior of PLA-based nanocomposites was determined using DSC measurements (Fig. 7). The melting temperature (T_m), melting enthalpy (ΔH_m), crystallization temperature (T_c) and crystallization enthalpy (ΔH_c) were determined for the neat PLA and the nanocomposites reinforced with different content of A-CNW. The neat PLA presented only a glass transition temperature close to 46°C, while did not show a clear T_m under the investigated conditions, this phenomenon was due to the almost "amorphous" state of PLA used in the study. In contrast, when APS modified CNW existing, PLA nanocomposites show a shoulder melting peak and a melting peaking around 141 and 150°C, together with a cold crystallization transition at T_c < 120°C. The presence of two distinct melting peaks or a melting peak and a
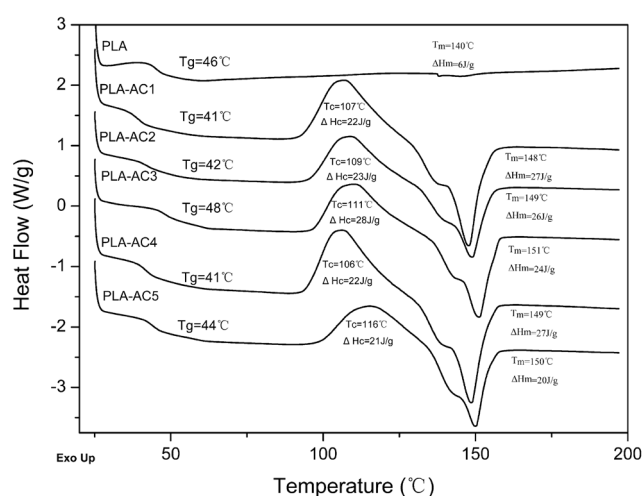

Fig. 7. DSC thermograms of neat PLA and PLA based composite films.

shoulder were well-known situations in the case of PLA, originating from the modification of PLA crystal growth [32]. It could be ascribed to the coexistence of two crystalline structure: less perfect-crystals (α′-form crystals), which had enough time to melt and recognize into crystals with greater structure perfection (α-form crystals) [33]. It was generally believed that the peak at the higher temperature was the melting peak produced by re-crystallization, and this pattern corresponded to a more stable melting process of the crystals [34]. This behavior can be explained by the nucleation effect by cellulose nanocrystals during the crystallization of PLA [35].

Incorporating APS modified CNW in the PLA matrix can be responsible for modifications in its crystallization by playing the role of nucleating agents. As shown in Fig. 7, the A-CNW content played an important role in determining the nucleating effect of PLA nanocomposites. The T_c of PLA-AC3 (1 wt %), PLA-AC4 (3 wt %), PLA-AC5 (5 wt %) resulted in a noticeable change from 116 to 106°C, which indicated the PLA nanocomposites with 2 % v/v APS/3 wt % CNW can crystallize much easier. Minor changes in T_g can be seen from 46 to 41°C when adding A-CNW (take the proportions of APS and the content of A-CNW into account), a behavior which persisted in the binary blend which may indicate a plasticization effect of the A-CNW toward PLA.

The decrease in the T_g suggested an increase of the mobility of polymer chains [36], which was also due to the miscible effect between PLA and A-CNW.

3.7. Scanning electron microscopy analysis

SEM micrographs of fractured surface of the PLA and its nanocomposites are presented in Fig. 8. The micrographs have been taken on the tensile fracture surface. From Fig. 8a the neat PLA showed the interlayer organization structure, then, the fracture surface became compact in presence of CNW which could be seen from Fig. 8b–8f. As shown in Fig. 8b, 8c and 8e, the nanocomposites present tough characteristics with increased APS concentration, which can be demonstrated with a rough fracture surface severely deformed PLA matrix. Some drawn deformation and wire drawing phenomenon were seen. The tensile behavior of the 2 % v/v APS/3 wt% CNW/PLA nanocomposite (Fig. 8e) should be attributed to the semi-brittle failure, which performed high tensile strength and relative good elongation.

For Fig. 8d, 8e and 8f, the fracture surface morphology of A-CNW/PLA nanocomposites with different content (1, 3 and 5 wt%) of CNW under the same APS adding amount (2 % v/v) was revealed. Compared to neat PLA, the surface of the PLA-AC3 (1 wt%) showed only roughness and
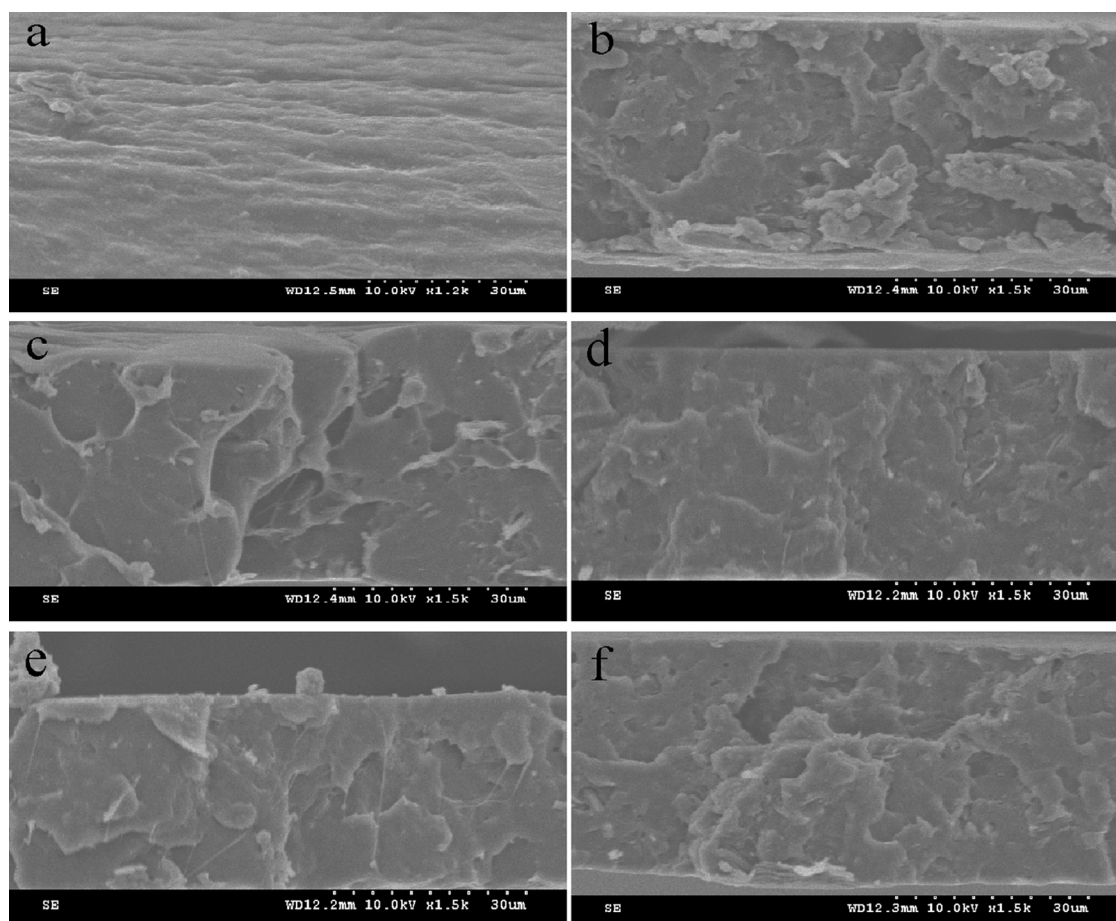

Fig. 8. Scanning electron microscope (SEM) photos of the fracture surfaces of the nanocomposite films (a) PLA; (b) PLA-AC1; (c) PLA-AC2; (d) PLA-AC3; (e) PLA-AC4; (f) PLA-AC5.

no wire drawing phenomenon, because it was difficult to form the network with low A-CNW content. But the nanocomposites with 5 wt% A-CNW (PLA-AC5) had a rougher surface compared to those with lower CNW contents. And the surface of PLA-AC5 showed in Fig. 8f, with A-CNW agglomeration, indicated that a relatively poor dispersion was achieved in composites with high CNW content [9]. From the SEM results, we can make a conclusion that the APS modified CNW improved the compatibility between CNW and PLA and both CNW and APS played an important role in improving the performance of PLA.

3.8. Dynamic mechanical thermal analysis

Fig. 9 shows the storage modules and tan delta as a function of temperature of the prepared nanocomposites. The materials showed a typical behavior for a semi-crystalline polymer, with a transition peak, related with T_g of PLA, at around 60°C for neat PLA and PLA based nanocomposites. As far as E' was concerned (Fig. 9A), we can observe that the storage modulus was significantly improved in the viscoelastic temperature region of the polymer for all nanocomposites. Thus, the CNW content had an important effect on improving the E' of the nanocomposites within the temperature region investigated in this study. For instance, E' determined at 25°C (glassy state) increased from 1030

MPa for neat PLA to more than 3400 MPa when loaded with 3 wt% CNW modified with 2% v/v APS (PLA-AC4), which supported the data obtained from tensile testing and the trend, as well as the values found to be comparable. The reinforcing effect provided by the chemically-modified CNW in the PLA matrix can be used to explain the increase in E' values. In addition, the concentration of APS did not affect the E' when APS adding amount was over 2% (v/v), which was due to the compatibility of PLA/A-CNW and the formation of a rigid percolating filler network interconnected by hydrogen bonds, while the content of CNW strongly affected the E' values of PLA nanocomposites. It can be explained that low CNW content could not be enough to form a network and was easy to cause fibrils aggregation with high content.

Fig. 9B shows how the addition of APS-modified CNW influenced the tan delta (related with the glass transition temperature) peak position of PLA. As can be seen from Fig. 9B, the tan delta peak of pure PLA was shifted to lower temperature with A-CNW adding into PLA matrix. The tan delta data are listed in Table 4. The peak position for PLA was at 60°C decreased to 54°C for the nanocomposites of 2% v/v APS/3 wt% CNW/PLA. Fig. 9B also shows the intensity of the tan delta peak increased with the addition of APS compared to neat PLA. The increase in storage modulus and negative shift in tan delta peak position can be attributed to
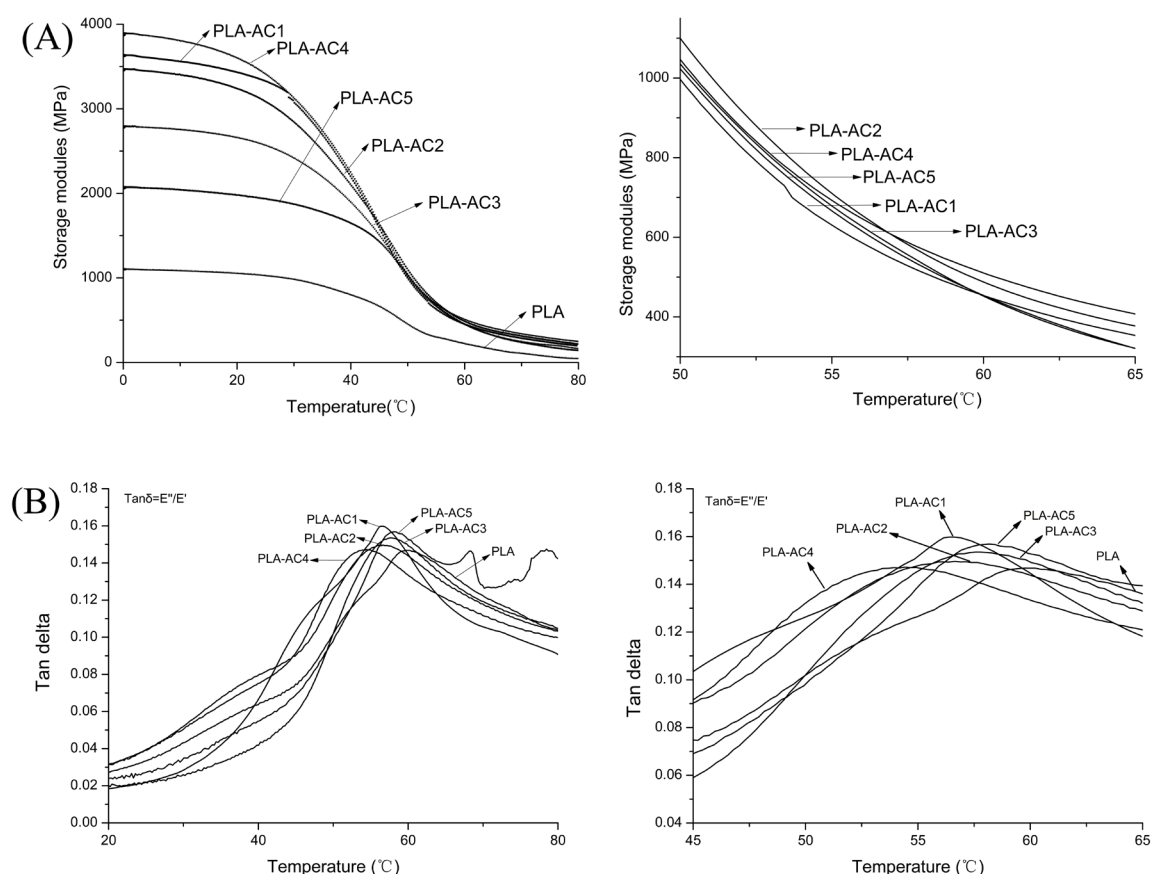

Fig. 9. DMA of PLA and PLA based nanocomposite films: (A) storage modulus and (B) tan δ curves.

Table 4
Storage modulus (E') and Tan delta of PLA based nanocomposite films (from 0 to 80°C, 5 µm, 1 Hz)

Samples	E' (MPa 25°C)	Tan delta (°C)
PLA	1030	60
PLA-AC1	3330	56
PLA-AC2	3100	56
PLA-AC3	2560	57
PLA-AC4	3420	54
PLA-AC5	1940	58

the network structure formed by A-CNW and strong interfacial interactions between A-CNW and PLA matrix, which can transfer energy from PLA to A-CNW, the similar results werre also found in the research of Wang et al [37].

4. Conclusion

It was demonstrated that the CNW could be well-dispersed in PLA matrix and had good interfacial interaction with PLA using solvent casting-evaporation process. The CNW with aspect ratio from 20 to 50, surface-modified with APS under aqueous suspension, kept their integrity and rod-like morphology. The coupling reaction had been successfully occurred between APS and CNW, which was evidenced by FTIR and XPS analysis. The mechanism of APS grafting onto the cellulose surface and A-CNW/PLA interfacial interaction was presented. It was noticed that the PLA/A-CNW composite film with 2% v/v APS and 3 wt % CNW showed the best tensile properties, the tensile strength and elongation increased significantly by 42.8% (50.6 MPa) and 108% (5.2%), in comparison with the neat PLA film whose tensile strength and elongation were 35.7 MPa and 2.5%, respectively. The fracture morphology study of PLA and its nanocomposite films showed that a relatively good dispersion was achieved. Thermal mechanical and thermal analyses showed that A-CNW acted as nano reinforcing agent for PLA matrix. DMA study indicated that the increased modulus, together with negative shift in tan delta peak positions, was attributed to the network structure formed by A-CNW and a layer of immobilized macromolecular chains resulting from stronger interactions at the cellulose/matrix interface.

Abbreviations

A-CNW	—	Aminopropyltriethoxysilane modified cellulose nanowisker
APS	—	Aminopropyltriethoxysilane
CNW	—	Cellulose nanowiskers
DMA	—	Dynamic mechanical analysis
DMAc	—	N, N-dimethylacetamide
DSC	—	Differential scanning calorimetry
FTIR	—	Fourier transform infrared spectroscopy
PLA	—	Polylactic acid
SEM	—	Scanning electron microscope
TEM	—	Transmission electron microscopy
XPS	—	X-ray photoelectron spectroscopy

References

[1] A.P. Johari, S.K. Kurmvanshi, S. Mohanty, S.K. Nayak, Influence of surface modified cellulose microfibrils on the improved mechanical properties of poly (lactic acid), Int. J. Biol. Macromol., 84 (2016) 329–339.

[2] I. Cacciotti, E. Fortunati, D. Puglia, J.M. Kenny, F. Nanni, Effect of silver nanoparticles and cellulose nanocrystals on electrospun poly (lactic) acid mats: Morphology, thermal properties and mechanical behavior, Carbonhyd. Polym., 103 (2014) 22–31.

[3] S.L. Yang, Z.H. Wu, W. Yang, M.B. Yang, Thermal and mechanical properties of chemical crosslinked polylactide (PLA), Polym. Test, 27 (2008) 957–963.

[4] R. Auras, B. Harte, S. Selke, An overview of polylactides as packaging materials, Macromol. Biosci., 4 (2004) 835–864.

[5] E. Fortunati, F. Luzi, D. Puglia, R. Petrucci, J.M. Kenny, L. Torre, Processing of PLA nanocomposites with cellulose nanocrystals extracted from Posidonia oceanica waste: Innovative reuse of coastal plant, Ind. Crop. Prod., 67 (2015) 439–447.

[6] T.J. Lu, S.M. Liu, M. Jiang, X.L. Xu, Y. Wang, Z.Y. Wang, J. Gou, D. Hui, Z.W. Zhou, Effects of modifications of bamboo cellulose fibers on the improved mechanical properties of cellulose reinforced poly (lactic acid) composites, Compos. Part B: Eng., 62 (2014) 191–197.

[7] S.Y. Cho, H.H. Park, Y.S. Yun, H.J. Jin, Cellulose nanowhisker-incorporated poly (lactic acid) composites for high thermal stability, Fiber. Polym., 14 (2013) 1001–1005.

[8] A. Kiziltas, B. Nazari, E.E. Kiziltas, D.J. Gardner, Y. Han, T.S. Rushing, Method to reinforce polylactic acid with cellulose nanofibers via a polyhydroxybutyrate carrier system, Carbonhyd. Polym., 140 (2016) 393–399.

[9] M. Jonoobi, J. Harun, A.P. Mathew, K. Oksman, Mechanical properties of cellulose nanofiber (CNF) reinforced polylactic acid (PLA) prepared by twin screw extrusion, Compos. Sci. Technol., 70 (2010) 1742–1747.

[10] Z. Xiong, S. Ma, L. Fan, Z. Tang, R. Zhang, H. Na, J. Zhu, Surface hydrophobic modification of starch with bio-based epoxy resins to fabricate high-performance polylactide composite materials, Compos. Sci. Technol., 94 (2014) 16–22.

[11] A. Iwatake, M. Nogi, H. Yano, Cellulose nanofiber-reinforced polylactic acid, Compos. Sci. Technol., 68 (2008) 2103–2106.

[12] T. Wang, L.T. Drzal, Cellulose-nanofiber-reinforced poly(lactic acid) composites prepared by a water-based approach, ACS. Appl. Mater. Inter., 4 (2012) 5079–5085.

[13] P. Qu, Y.T. Zhou, X. Zhang, S. Yao, L.P. Zhang, Surface modification of cellulose nanofibrils for poly(lactic acid) composite application, J. Appl. Polym. Sci., 125 (2012) 3084–3091.

[14] A. Arbelaiz, B. Fernandez, J. Ramos, A. Retegi, R. Llano-Ponte, I. Mondragon, Mechanical properties of short flax fibre bundle/polypropylene composites: Influence of matrix/fibre modification, fibre content, water uptake and recycling, Compos. Sci. Technol., 65 (2005) 1582–1592.

[15] M. Murariu, A.L. Dechief, R. Ramy-Ratiarison, Y. Paint, J.M. Raquez, P. Dubois, Recent advances in production of poly(lactic acid) (PLA) nanocomposites: A versatile method to tune crystallization properties of PLA, Nanocomposites, 1 (2015) 71–82.

[16] A. Orue, A. Jauregi, C. Peña-Rodriguez, J. Labidi, A. Eceiza, A. Arbelaiz, The effect of surface modifications on sisal fiber properties and sisal/poly (lactic acid) interface adhesion, Compos. Part B: Eng., 73 (2015) 132–138.

[17] J. Araki, M. Wada, S. Kuga, Steric stabilization of a cellulose microcrystal suspension by poly(ethylene glycol) grafting, Langmuir, 17 (2001) 21–27.

[18] N. Lin, G. Chen, J. Huang, A. Dufresne, P.R. Chang, Effects of polymer-grafted natural nanocrystals on the structure and mechanical properties of poly(lactic acid): A case of cellulose whisker-graft-polycaprolactone, J. Appl. Polym. Sci., 113 (2009) 3417–3425.

[19] A. Pei, Q. Zhou, L.A. Berglund, Functionalized cellulose nano-crystals as biobased nucleation agents in poly(l-lactide) (PLLA) – Crystallization and mechanical property effects, Compos. Sci. Technol., 70 (2010) 815–821.

[20] G. Chen, A. Dufresne, J. Huang, P.R. Chang, A novel ther-moformable bionanocomposite based on cellulose nanocrys-tal-graft-poly(ε-caprolactone), Macromol. Mater. Eng., 294 (2009) 59–67.

[21] A. Rider, D. Arnott, Boiling water and silane pre-treatment of aluminium alloys for durable adhesive bonding, Int. J. Adhes. Adhes., 20 (2000) 209–220.

[22] E. Robles, I. Urruzola, J. Labidi, L. Serrano, Surface-modified nano-cellulose as reinforcement in poly(lactic acid) to conform new composites, Ind. Crop. Prod., 71 (2015) 44–53.

[23] F. Bauer, H.J. Gläsel, U. Decker, H. Ernst, A. Freyer, E. Hart-mann, V. Sauerland, R. Mehnert, Trialkoxysilane grafting onto nanoparticles for the preparation of clear coat polyacrylate systems with excellent scratch performance, Prog. Org. Coat., 47 (2003) 147–153.

[24] H. Cui, M.R. Kessler, Glass fiber reinforced ROMP-based bio-renewable polymers: Enhancement of the interface with silane coupling agents, Compos. Sci. Technol., 72 (2012) 1264–1272.

[25] A. Zafar, J.S. Thomsen, R. Sodhi, R. Goacher, D. Kubber, X-ray photoelectron spectroscopy and time-of-flight secondary ion mass spectrometry characterization of aging effects on the mineral fibers treated with aminopropylsilane and quater-nary ammonium compounds, Surf. Interface. Anal., 44 (2012) 811–818.

[26] R.A. Khan, S. Salmieri, D. Dussault, J. Uribe-Calderon, M.R. Kamal, A. Safrany, M. Lacroix, Production and properties of nanocellulose-reinforced methylcellulose-based biodegrad-able films, J. Agr. Food Chem., 58 (2010) 7878–7885.

[27] J. Lu, P. Askeland, L.T. Drzal, Surface modification of micro-fibrillated cellulose for epoxy composite applications, Poly-mer., 49 (2008) 1285–1296.

[28] M. Abdelmouleh, S. Boufi, M. Belgacem, A. Duarte, A.B. Salah, A. Gandini, Modification of cellulosic fibres with function-alised silanes: development of surface properties, Int. J. Adhes. Adhes., 24 (2004) 43–54.

[29] G. Stiubianu, C. Racles, M. Cazacu, B.C. Simionescu, Sili-cone-modified cellulose. Crosslinking of cellulose acetate with poly [dimethyl (methyl-H) siloxane] by Pt-catalyzed dehydro-genative coupling, J. Mater. Sci., 45 (2010) 4141–4150.

[30] K. Missoum, M.N. Belgacem, J.P. Barnes, M.C. Brochier-Salon, J. Bras, Nanofibrillated cellulose surface grafting in ionic liq-uid, Soft Matter, 8 (2012) 8338–8349.

[31] L. Matuana, J. Balatinecz, C. Park, R. Sodhi, X-ray photoelec-tron spectroscopy study of silane-treated newsprint-fibers, Wood. Sci. Technol., 33 (1999) 259–270.

[32] J.M. Raquez, Y. Murena, A.L. Goffin, Y. Habibi, B. Ruelle, F. DeBuyl, P. Dubois, Surface-modification of cellulose nanow-hiskers and their use as nanoreinforcers into polylactide: a sustainably-integrated approach, Compos. Sci. Technol., 72 (2012) 544–549.

[33] A.N. Frone, S. Berlioz, J.F. Chailan, D.M. Panaitescu, Morphol-ogy and thermal properties of PLA–cellulose nanofibers com-posites, Carbohyd. Polym., 91 (2013) 377–384.

[34] L. Wang, Y.N. Wang, Z.G. Huang, Y.X. Weng, Heat resistance, crystallization behavior, and mechanical properties of poly-lactide/nucleating agent composites, Mater. Design, 66 (2015) 7–15.

[35] A.L. Goffin, J.M. Raquez, E. Duquesne, G. Siqueira, Y. Habibi, A. Dufresne, P. Dubois, From interfacial ring-opening polym-erization to melt processing of cellulose nanowhisker-filled polylactide-based nanocomposites, Biomacromolecules, 12 (2011) 2456–2465.

[36] H. Liu, D. Liu, F. Yao, Q. Wu, Fabrication and properties of transparent polymethylmethacrylate/cellulose nanocrystals composites, Bioresour. Technol., 101 (2010) 5685–5692.

[37] D. Wang, J. Yu, J. Zhang, J. He, J. Zhang, Transparent bionano-composites with improved properties from poly (propylene carbonate) (PPC) and cellulose nanowhiskers (CNWs), Com-pos. Sci. Technol., 85 (2013) 83–89.